# Neutron Scattering Estimates of the Effect of Charge on the Micelle Structure in Aqueous Polyelectrolyte Diblock Copolymer Solutions

**W. Groenewegen,[†] S. U. Egelhaaf,[‡] A. Lapp,[§] and J. R. C. van der Maarel*[,†]**

*Leiden Institute of Chemistry, Gorlaeus Laboratories, Leiden University, PO Box 9502, 2300 RA Leiden, The Netherlands, Department of Physics and Astronomy, JCMB, University of Edinburgh, Edinburgh EH9 3JZ, United Kingdom, and Laboratoire Léon Brillouin, CE de Saclay, 91191 Gif-sur-Yvette Cedex, France*

*Received December 20, 1999; Revised Manuscript Received February 21, 2000*

ABSTRACT: The dimension of spherical micelles of the diblock copolymer poly(styrene-*block*-acrylic acid) [PS(20)-*b*-PA(85)] was investigated as a function of the degree of ionization of the polyelectrolyte in the coronal layer. To describe the structural arrangement of the blocks, the partial structure factors pertaining to PS−PS and PA−PA density correlations as well as the composition structure factor were obtained with small-angle neutron scattering and contrast matching in water. The PS blocks form a densely packed spherical core with a radius 4.5 nm and an aggregation number ∼100; the core structure does not depend on the corona charge to a significant degree. The extension of the PA chains in the coronal layer, and, hence, the micelle radius, are found to be highly sensitive to the degree of ionization. At full ionization, the PA chains are almost fully stretched with a density scaling proportional to the inverse second power of the radius away from the core. For lower charge fraction, the results are interpreted in terms of scaling theory for star-branched polyelectrolytes, including the effects of charge annealing. The dimension of the micelles was found to be controlled by the balance of the elastic, conformational, stretching forces and the osmotic pressure exerted by the counterions trapped within the corona.

## Introduction

Amphiphilic diblock copolymers with a polyelectrolyte block comprise two linearly attached moieties: a charged and a hydrophobic chain part. The hydrophobic attachment provides a mechanism for bringing the copolymers together, and new mesoscopic structures are established. The self-organized structures consist of units of mesoscopic size, which are large compared to the molecular dimensions. The self-association behavior is of unusual complexity due to the interplay between charge and hydrophobic interactions and packing effects. Polyelectrolyte diblock copolymers have considerable potential in industrial applications due to the increased need of water-supported systems.

Major factors controlling mesoscopic order are charge, ionic strength, and the size of the hydrophobic attachment. For ionic diblocks of poly(styrene-*block*-sodium acrylate) (PS-*b*-NaPA) with a polyelectrolyte (NaPA) block length smaller than the length of the polystyrene (PS) block moiety, a multitude of different "crew-cut" mesoscopic structures has been observed by Eisenberg and co-workers.[1−3] These structures include hexagonal wormlike cylinders, lamellae, and (compound) vesicles. If the length of the core-forming block is comparable to or smaller than the length of the corona-forming block, it was observed that the copolymers associate to form spherical micelles with a hydrophobic core and a polyelectrolyte corona. It should be noted, however, that due to the high glass temperature (363 K) of the PS block, the observed structures refer to frozen metastable states, and they depend on how the samples are prepared. Once the mesoscopic structures are formed after cooling below the glass temperature, the order is fixed. A few studies considered ionic copolymers with a soft hydrophobic block with a glass transition below ambient temperature.[4,5] It was seen that these soft micelles fuse into vesicles and a fractal network, and eventually the solution separates into a dilute micellar phase and a gel phase with increasing polymer and salt concentration.[6,7]

The critical micelle concentrations of PS-*b*-NaPA dispersed in water were reported as a function of block lengths and salt content and explained on the basis of the scaling of the star and some mean-field models.[8,9] For spherical micelles, hydrodynamic diameters and scaling relations for the core size were derived from dynamic light scattering and transmission electron microscopy (TEM), respectively.[10] These results show that, in the absence of salt and high pH, the ionized form of the poly(acrylic acid) (PAA) chains in the coronal layer have a highly extended conformation. A near-perfect rodlike stretching (with a scattered intensity $\sim q^{-1}$)[11] of the arms has also been reported for micelles formed by poly(*tert*-butylstyrene-*block*-sodium styrenesulfonate) (PtBS-*b*-NaPSS) copolymers.[12] This behavior is strikingly different from the situation for uncharged spherical polymer brushes and/or star-branched polymers, where the chains take a more compact coiled conformation.[13−17] The previously investigated systems contain polyelectrolyte blocks with rather high degrees of ionization (or sulfonation), and as far as we are aware, the transition from the neutral to the charged spherical brush has not been studied in great detail. It is therefore of interest to investigate the conformation of the corona as a function of its charge and to explore to what extent the polyelectrolyte block becomes stretched at high degree of ionization.

PAA is a weak acid, and its degree of ionization can be adjusted by titration of the carboxyl groups. We have investigated spherical micelles of PS-*b*-PA, in which the corona charge is tuned between almost zero (there is

[†] Leiden University.
[‡] University of Edinburgh.
[§] Laboratoire Léon Brillouin.
* Author for correspondence.

10.1021/ma992116p CCC: $19.00 
Published on Web 04/13/2000

always some residual charge due to autodissociation) and full charge where every segment carries an ionized group. In the present contribution, the acronym PA denotes the poly(acrylic acid) block irrespective degree of neutralization. The ionization process is monitored with infrared (IR) spectroscopy, and the morphology of the self-assembled structures was checked with TEM. Detailed structural information is inferred from small-angle neutron scattering (SANS). The scattering is sensitive to the set of spatial Fourier transforms of the solute density correlation functions, i.e., the partial structure factors.[18] The potential of this approach lies in its spatial resolution together with contrast variation to blank or highlight certain components in the complex mixture of copolymer blocks, solvent, and counterions.[19,20] We will determine the individual structure factors pertaining to the density correlations among the PS and PA blocks as well as the composition structure factor. The composition structure factor describes the spatial fluctuation of the *difference* in PS and PA block densities and is particularly sensitive to the ordering of the blocks and the intramicelle structure.

The aggregation number (i.e., the number of self-assembled copolymers per micelle), core size, and physical extent of the corona are derived from the scattering behavior. For this purpose, the structure factors are interpreted with radial density profiles pertaining to either a densely packed core or a corona with a certain chain statistics. Indeed, it is seen that the core has a spherical shape, and its dimension does not depend on the charge and/or copolymer concentration to a significant degree. For a description of the corona, mean-field and scaling theories of spherical polyelectrolyte brushes and/or star-branched polyelectrolytes are available in the literature.[21−24] In the present contribution, the corona chain statistics will be gauged from the scaling approaches including the effects of the elastic (conformational) stretching forces and the osmotic pressure exerted by the counterions trapped inside the brush (osmotic regime).[25−27] At high degree of ionization, we recover the behavior of a highly extended corona with a scaling of the segment density proportional to the inverse second power of the radius. At lower charge fraction, the corona shrinks, and the effect of charge annealing and migration of the charges toward the outer corona region becomes apparent.[27] Finally, the derived dimension of the micelles as a function of their charge is interpreted with the scaling result for polyelectrolyte stars in the osmotic regime.[25,26]

## Theory

**Structure Factors.** For a diblock $A(N_A)$-*b*-$B(N_B)$ copolymer solution, with $N_A$ and $N_B$ the number of monomers of block *A* and *B*, respectively, it is convenient to consider the blocks as the elementary scattering units.[28] Every block *A* is attached to a *B* block, and hence, the macroscopic block concentrations exactly match the copolymer concentration $\rho_A = \rho_B = \rho$. The coherent part of the solvent corrected SANS intensity reads

$$I(q)/\rho = \bar{b}_A{}^2 N_A{}^2 S_{AA}(q) + 2\bar{b}_A\bar{b}_B N_A N_B S_{AB}(q) + \bar{b}_B{}^2 N_B{}^2 S_{BB}(q) \quad (1)$$

with the block *monomer* scattering length contrasts $\bar{b}_A$ and $\bar{b}_B$, respectively. In an $H_2O/D_2O$ solvent mixture, the scattering length contrast is given by

$$\bar{b}_i = b_i - b_s\bar{v}_i/\bar{v}_s,$$
$$b_s = X(D_2O)b_{D_2O} + (1 - X(D_2O))b_{H_2O} \quad (2)$$

with $X(D_2O)$ the $D_2O$ mole fraction. The monomer $i = A$, *B* and solvent *s* have scattering lengths $b_i$ and $b_s$ and partial molar volumes $\bar{v}_i$ and $\bar{v}_s$, respectively. In our experiments the structure factors are obtained from the intensities by contrast variation in the water, i.e., by adjusting the solvent scattering lengths $b_s$.

The partial structure factors $S_{ij}(q)$ are the spatial Fourier transforms of the *block* density correlation functions

$$S_{ij}(q) = \frac{1}{\rho}\int_V \mathrm{d}\vec{r}\ \exp(-i\vec{q}\cdot\vec{r})\langle\rho_i(0)\ \rho_j(\vec{r})\rangle \quad (3)$$

It is of particular interest to construct the composition structure factor

$$S_{AA}(q) - 2S_{AB}(q) + S_{BB}(q) = \frac{1}{\rho}\int_V \mathrm{d}\vec{r}\ \exp(-i\vec{q}\cdot\vec{r})\langle[\rho_A(0) - \rho_B(0)][\rho_A(\vec{r}) - \rho_B(\vec{r})]\rangle \quad (4)$$

This structure factor displays a maximum at wavelengths of the order of the inverse correlation distance between the *A* and *B* blocks. In the $q \to 0$ limit the composition structure factor goes to zero because macroscopic phase separation is impossible due to the fact that every *A* block is chemically connected to a *B* block.

In a selective solvent, the copolymers form spherical aggregates with a hydrophobic *A* block core and a polyelectrolyte *B* block corona. For a monodisperse system and if the corona structure is invariant to fluctuations in intermicelle separation, the structure factor eq 3 takes the form[18]

$$S_{ij}(q) = \frac{1}{N_{ag}} F_i(q)\ F_j(q)\ S_{cm}(q) \quad (5)$$

with the micelle aggregation number $N_{ag}$, the form factor amplitude $F_i(q)$, and the micelle center-of-mass structure factor $S_{cm}(q)$. In the absence of interactions between the micelles and/or at sufficiently high values of momentum transfer $S_{cm}(q)$ reduces to unity. The form factor amplitude $F_i(q)$ can be expressed in terms of the *radial* core ($i = A$) or corona ($i = B$) density $\rho_i(r)$

$$F_i(q) = \int_{V_{micelle}} \mathrm{d}\vec{r}\ \exp(-i\vec{q}\cdot\vec{r})\rho_i(\vec{r}) = \int \mathrm{d}r\ \sin(qr)/(qr)4\pi r^2\rho_i(r) \quad (6)$$

The scattering amplitudes are normalized to $N_{ag}$ at $q = 0$. With eq 5, the composition structure factor eq 4 takes the form

$$S_{AA}(q) - 2S_{AB}(q) + S_{BB}(q) = \frac{1}{N_{ag}}[F_A(q) - F_B(q)]^2 S_{cm}(q) \quad (7)$$

The factorization of the structure factors into the intramicelle form factor amplitudes $F_i(q)$ and the intermicelle center-of-mass structure factor $S_{cm}(q)$ according to eq 5 is important in recognizing certain relations between the different partial structure factors and the data analysis procedure. The center-of-mass structure factor $S_{cm}(q)$ is positive definite, since it represents a scattered intensity (i.e., a squared amplitude). The

intensities eq 1 can now be expressed in terms of two factors $u_i(q)$ rather than three partial structure factors $S_{ij}(q)$ ($i, j = A, B$):

$$I(q)/\rho = [\bar{b}_A N_A u_A(q) + \bar{b}_B N_B u_B(q)]^2,$$
$$u_i(q) = [S_{cm}(q)/N_{ag}]^{1/2} F_i(q) \quad (8)$$

As will be shown below, explicit use of eq 5 in the data analysis procedure according to eq 8 (and, hence, with a concomitant reduction in number of adjustable parameters) results in improved statistical accuracy in the derived structure factors.

**Scattering Amplitudes**. In the case of dense core packing, the radial $A$ block density is uniform for $0 \le r \le r_c$ and given by $\rho_A(r) 4\pi r_c^3/3 = N_{ag}$ and 0 for $r > r_c$, with $r_c$ the core radius. For such uniform profile, the core form factor amplitude takes the form

$$F_A(q) = N_{ag} 3(\sin(qr_c) - qr_c \cos(qr_c))/(qr_c)^3 \quad (9)$$

Expressions for the scattering amplitude of Gaussian chains with constant density in the coronal layer (and the interference with the spherical core) are available in the literature.[29] However, due to the relatively small core size and the mutual segment repulsion induced by the charge, the density in the coronal layer is nonuniform and varies along with the radius away from the core. To describe the corona structure, we will adopt an algebraic radial $B$ block density profile

$$\rho_B(r) = \rho_B(r_c)\,(r/r_c)^{-\alpha} \qquad r_c \le r \le r_o \quad (10)$$

where corona chain statistics determines the value of $\alpha$ and $\rho_B(r_c)$ is the density at the core−corona interface. The latter interfacial density is related to the outer micelle radius $r_o$ through the normalization requirement (i.e., by integration of the radial profile)

$$4\pi\rho_B(r_c)(r_o^{3-\alpha} r_c^{\alpha} - r_c^3)/(3 - \alpha) = N_{ag} \quad (11)$$

We will calculate the scattering amplitude eq 6 with algebraic profile eq 10 by numeric integration, although complex analytical expressions are available.[30]

The algebraic profile eq 10 accounts for the *average* corona density scaling and neglects corona chain *fluctuations*. The effect of fluctuations on the scattering behavior is important when the momentum transfer is of the order of the intermolecular correlation distance within the corona. Furthermore, they contribute to the corona structure factor $S_{BB}$ only; the cross term $S_{AB}$ is unaffected due to the heterodyne interference between the amplitudes scattered by the homogeneous core and heterogeneous corona.[31,32]

**Corona Chain Statistics.** The value of the density scaling exponent $\alpha$ is determined by the statistics of the polyelectrolyte block. For a condensed globular state the density is uniform with $\alpha = 0$ (this situation applies to the core). The value $\alpha = 2$ is relevant when the corona charge is sufficiently high to induce a linear chain configuration with uniform mass per unit length. This can be due to either full stretching of the chains or the formation of radial strings of blobs of uniform size. At zero charge a Daoud−Cotton expanding blob model might apply.[13] Here, $\alpha$ takes the value 1 or $^4/_3$ without ($\nu = {}^1/_2$) or with ($\nu = {}^3/_5$) chain volume interactions, respectively. For low corona charge, a two-region model has been proposed to describe the density scaling.[24,26,27] In the inner corona region the blobs expand (with $\alpha$ of the order of unity) until a critical size is reached; for larger radial distances the blob size remains constant ($\alpha = 2$). The value of the density scaling exponent exceeds two if the blob size *decreases* with increasing distance away from the core. As will be discussed below, the latter phenomenon might occur due to the effects of charge annealing.

Scaling expressions for the size and the transition distance between the expanding and constant blob size regions have been derived for star-branched polyelectrolytes with a quenched charge distribution.[26,27] These starlike polymers can also serve as a model for spherical polyelectrolyte diblock copolymer micelles; the presence of the hydrophobic core has no effect on the scaling results. Without the presence of supporting electrolyte, two different classes of star-branched polyelectrolytes exist. When the fraction $f_q$ of ionized groups is very small, the electrostatic screening length is much larger than the micelle size, and hence, inside the corona there is no screening of Coulomb interaction. With increasing $f_q$ the majority of the counterions are trapped within the corona, and now, the concomitant osmotic pressure gives the main contribution to the corona stretching force. The transition between the unscreened and the screened, osmotic, micelle occurs at a critical charge fraction

$$f_q \sim (a_B/Q)^{1/\nu} N_{ag}^{-1/\nu} \quad (12)$$

with $Q$ the Bjerrum length (0.7 nm at 298 K) and $a_B$ the distance between neighboring links in the $B$ block. For micelles with a large aggregation number, the unscreened regime can only be observed if $f_q \ll 1$. Because of the large aggregation number (of the order of 100), most, if not all, of our samples are in the osmotic regime, and accordingly, we will only summarize the results for osmotic micelles.[26,27] As a surprising result, the outer radius of the osmotic micelle does not depend on the aggregation number and scales with the corona charge fraction according to

$$r_o \sim N_B a_B f_q^{1-\nu} \quad (13)$$

Because of the osmotic pressure of the trapped counterions, in the outer region of the corona the blob size $\xi$ is constant and is given by

$$\xi \sim a_B f_q^{-\nu} \quad (14)$$

The crossover radial distance $r^*$ between the expanding and constant blob size regions is of the order of $r^* \sim a_B f_q^{-\nu} N_{ag}^{1/2}$. With increasing corona charge fraction $f_q$, the expanding blob size region shrinks and eventually vanishes if $r^*$ becomes of the order of the core radius $r_c$. Concurrently, due to the osmotic pressure of the counterions, the corona becomes uniformly extended ($\alpha = 2$) and can be envisioned as strings of blobs of constant size given by eq 14. The presence of the core just limits the range over which the corona blobs are allowed to expand. This is in contrast to the situation of star-branched polyelectrolytes, where the expanding blob region extends right to the center of the star.

However, PA is a weak acid, and at low fraction of ionized monomers ($f_q \ll 1$), the effects of charge annealing might be important.[27] In the most simple approximation, the *local* charge fraction $f_q(r)$ is determined by the (presumably $r$-independent) ionization constant

$K$ and the mass action law $K = \rho(r)f_q(r)^2/(1 - f_q(r)) \approx \rho(r)f_q(r)^2$. Because of the dissociation and recombination balance, the charge fraction is now no longer constant and increases with increasing $r$ according to $f_q(r) \sim r^{2/(1+\nu)}$. A remarkable result of this charge annealing effect is that the blob size $\xi$ *decreases* with increasing distance away from the core

$$\xi \sim a_B r^{-2\nu(1+\nu)} \tag{15}$$

and the density scaling exponent $\alpha$ takes the value $^8/_3$ or $^5/_2$ without ($\nu = {}^1/_2$) or with ($\nu = {}^3/_5$) volume interactions, respectively.

## Experimental Section

**Polyelectrolyte Block Copolymer.** PS-*b*-NaPA was purchased from Polymer Source Inc., Dorval, Canada. According to the manufacturer, the number-average molecular weights $M_n$ of the PS and NaPA blocks are 2000 and 11 450, respectively. The molecular weight polydispersity $M_w/M_n$ ratio of the copolymer is 1.06. The PS block molecular weight was determined by size exclusion chromatography, whereas the degree of polymerization of the PA block was calculated from the ratio of the peak areas of the aromatic to that of the aliphatic protons in the NMR spectrum of the poly(styrene-*b*-*tert*-butyl acrylate) precursor. PS-*b*-NaPA was brought in the PS-*b*-PAA acid form by dissolving it in 0.1 M HCl and extensive dialysis against water (purified by a Millipore system with conductivity less than $1 \times 10^{-6}\ \Omega^{-1}\ cm^{-1}$). The residual sodium content in PS-*b*-PAA was checked by atomic absorption spectroscopy and was less than 0.001. Solutions were prepared by dissolving freeze-dried PS-*b*-PAA in pure water and/or $D_2O$ at 350 K under continuous stirring for 6 h. Furthermore, to break up clusters of micelles (see below), the solutions were sonicated (Bransonic 5200) for 30 min at room temperature. The sonication power was relatively low (190 W) and, hence, without risk of damage or decomposition of the block copolymers. In this work, concentrations are given in either grams of copolymer or polyelectrolyte block monomer (PA) per $dm^3$. Copolymer concentrations were determined by potentiometric titration of the PAA block with NaOH (Titrisol, Merck). The neutralization process was followed with IR spectroscopy. For this purpose, spectra of six solutions in $D_2O$ with polyelectrolyte block monomer concentration 0.15 mol of PA/$dm^3$ and degrees of neutralization DN = 0, 0.2, 0.4, 0.6, 0.8, and 1 were recorded with a Biorad FTS 175. The degree of neutralization is the molar ratio of (added) alkali and polyacid monomer.

**Electron Microscopy.** To study the morphology of the aggregates, TEM was done on 4 g/L PS-*b*-PA solutions at degrees of neutralization DN = 0 and 1. A droplet was deposited on a freshly cleaved mica surface, and after evaporation of the solvent, the surface was shadowed with platinum (2.5 nm thickness) at an angle of 30°. For film strengthening, a 30 nm carbon layer was evaporated onto the surface. For freeze-fracture microscopy, block copolymer solutions were suspended in Vaseline and rapidly frozen ($10^5$ K/s) by immersing in liquid propane at 93 K. The frozen samples were fractured with a freeze-fracture device (Balzers BAF400) at 123 K and a pressure of $2.5 \times 10^{-5}$ Pa. Next, the fresh surfaces were shadowed and strengthened with platinum and carbon, respectively. Finally, after thawing, the suspensions were dissolved in a chloroform/methanol mixture, and the replicas were put on a MESH 400 grid. The replicas were examined with a Philips EM 410 microscope, and the images were recorded with a 31 000× magnification factor.

**Scattering.** For neutron scattering eight sets of samples were prepared. Six sets were made with degrees of neutralization DN = 0, 0.04, 0.1, 0.35, 0.6, and 1 and polyelectrolyte block monomer concentration 0.093 mol of PA/$dm^3$. The remaining two sets contained solutions with DN = 0 and 1 but a factor of 2 diluted polymer concentration 0.046 mol of PA/$dm^3$. The polyelectrolyte block charge was set by titration with NaOH or NaOD in $D_2O$. For contrast variation, all solutions were prepared in $H_2O$ and $D_2O$ and subsequently mixed by weight to obtain four different $H_2O/D_2O$ solvent compositions. The solvent compositions were checked by the values for transmission and with IR spectroscopy. Scattering length contrasts were calculated with eq 2 and the parameters in Table 1 and are collected in Table 2. For each degree of neutralization, the corona scattering length contrast has been calculated by taking the relevant average of the PAA and NaPA contrast parameters, $\bar{b}_{PAA}$ and $\bar{b}_{NaPA}$, respectively. Reference solvent samples with matching $H_2O/D_2O$ composition were also prepared. Standard quartz sample containers with 0.1 cm (for samples in pure $H_2O$) or 0.2 cm path length were used.

SANS experiments were done with the D22 diffractometer, situated on the cold source of the high neutron flux reactor at the Institute Max von Laue−Paul Langevin (ILL), Grenoble, France. The temperature was kept at 293 K. Samples were measured with two different instrument configurations. A wavelength of 0.8 nm was selected, and the effective distances between the sample and the planar square multidetector (S−D distance) were 1.4 and 14.5 m, respectively. This allows for a momentum transfer range of 0.03−4.7 $nm^{-1}$. The instrument resolution is given by a 10% wavelength spread and an uncertainty in angle $\Delta\theta = 1.2 \times 10^{-3}$ and $3.4 \times 10^{-3}$ for the 14.5 and 1.4 m S−D distance, respectively. The uncertainty in angle comprises contributions from the collimation, sample aperture, and detector cell size. The counting times were approximately 1 h/sample. Data correction allowed for sample transmission and detector efficiency. The efficiency of the detector was taken into account with the scattering of $H_2O$. Absolute intensities were obtained by reference to the attenuated direct beam, and the scattering of the pure solvent with the same $H_2O/D_2O$ composition was subtracted. Finally, the intensities were corrected for a small solute incoherent contribution.

**Table 1. Partial Molar Volumes and Scattering Lengths[a]**

| solute | $\bar{\nu}_i$ ($cm^3$/mol) | $b_i$ ($10^{-12}$ cm) |
|---|---|---|
| PAA | 47.6 | $1.658 + 1.041X(D_2O)$ |
| NaPA | 33.8 | 2.396 |
| PS | 99 | 2.326 |
| $H_2O$ | 18 | −0.168 |
| $D_2O$ | 18 | 1.915 |

[a] The PAA and NaPA partial molar volumes were taken from ref 39. $X(D_2O)$ denotes the $D_2O$ mole fraction (effect of exchangeable hydrogen). The polymer data refer to the monomeric unit.

**Table 2. Scattering Length Contrast in $10^{-12}$ cm**

| solvent | $\bar{b}_{PS}$ | $\bar{b}_{PAA}$ | $\bar{b}_{NaPA}$ |
|---|---|---|---|
| $H_2O$ | 3.24 | 2.10 | 2.71 |
| 28% $D_2O$ | 0.02 | 0.83 | 1.60 |
| 47% $D_2O$ | −2.60 | −0.20 | 0.69 |
| $D_2O$ | −8.10 | −2.36 | −1.20 |

## Results and Discussion

**Polyelectrolyte Block Ionization.** The ionization of the poly(acrylic acid) block can be monitored with IR spectroscopy. In the range 1500−1800 $cm^{-1}$ two bands can be distinguished. As displayed in Figure 1, the charge neutralization results in the appearance of the asymmetric $COO^-$ stretching band at 1570 $cm^{-1}$ with a concurrent disappearance of the C═O stretching band around 1700 $cm^{-1}$. The relative peak intensities are displayed in the inset of Figure 1. To a good approximation, the peak intensities are proportional to the molar ratio of (added) alkali and polyacid monomer (i.e., the degree of neutralization DN). The $COO^-$ and the C═O peak intensities vanish in the limit of no (DN = 0) and full (DN = 1) charge neutralization, respectively. For fully neutralized samples, every acid group of the polyelectrolyte block is ionized. Without the addition of alkali (DN = 0), the copolymer is still weakly charged

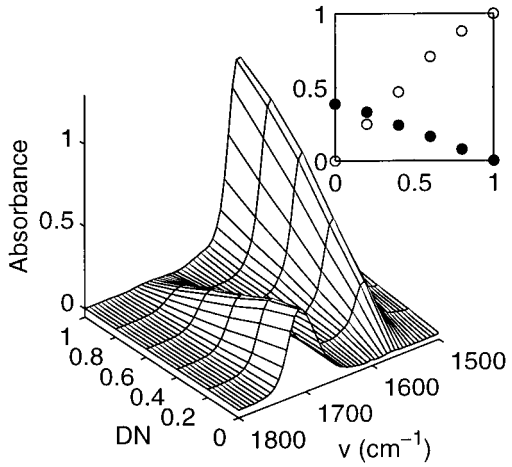


**Figure 1.** IR spectra versus degree of neutralization DN from 0.15 mol of PA/dm$^3$ PS-*b*-PA solutions. The inset displays the integrated peak intensities of the $COO^-$ (1570 cm$^{-1}$, open symbols) and C═O (1700 cm$^{-1}$, closed symbols) asymmetric and symmetric stretching bands, respectively, normalized to the $COO^-$ band at DN = 1.

due to the autodissociation of the COOH group. However, as judged from potentiometry, the degree of autodissociation is of the order $10^{-3}$ and is beyond the accuracy of the IR experiment.[33] Accordingly, the polyelectrolyte block charge fraction $f_q$ can be tuned between almost zero and unity by adjusting the degree of neutralization DN.

**Association Morphology**. It is known that in aqueous PS-*b*-PA solutions the copolymer micelles cluster and form extended association structures.[9] Accordingly, among others, the viscosity depends on the way the samples are prepared. We found that the clusters can be broken up by keeping the solution at 360 K for over 6 h, followed by sonication for 30 min at room temperature. It was checked that after these heating and sonication periods the viscosity has dropped to a constant value. The morphology of the self-assembled structures and the effectiveness of the sample preparation procedure were examined with TEM.

Figure 2 shows carbon replicas of solutions with full (DN = 1) and almost zero (DN = 0) polyelectrolyte block charge. The DN = 1 sample was imaged directly (after evaporation of the solvent from the grid, film strengthening, and shadowing), whereas the DN = 0 replica was obtained with freeze-fracture techniques. For both cases, the replicas show homogeneously dispersed and well-separated individual spherical micelles. With the ionization of the polyelectrolyte block, the diameter of the micelles increases due to the concomitant corona expansion from ∼30 to ∼50 nm. The estimated diameters are in the range of those determined by SANS (see below), and the TEM micrographs are, hence, sensitive to the physical extent of the corona. This is not a surprising result, because the carbon/platinum film covers the whole micelle and not only the core (or the freeze-fractured surface). We have nevertheless refrained from further analysis of the TEM micrographs, because of the uncertainties in size estimation introduced by the fracturing and shadowing procedures. The morphology of the individual micelles is further investigated with SANS and contrast matching in the water. As will be shown below, SANS provides an in situ measurement technique without the risk of damage and/or micelle deformation caused by the TEM drying or freeze-fracturing procedures.

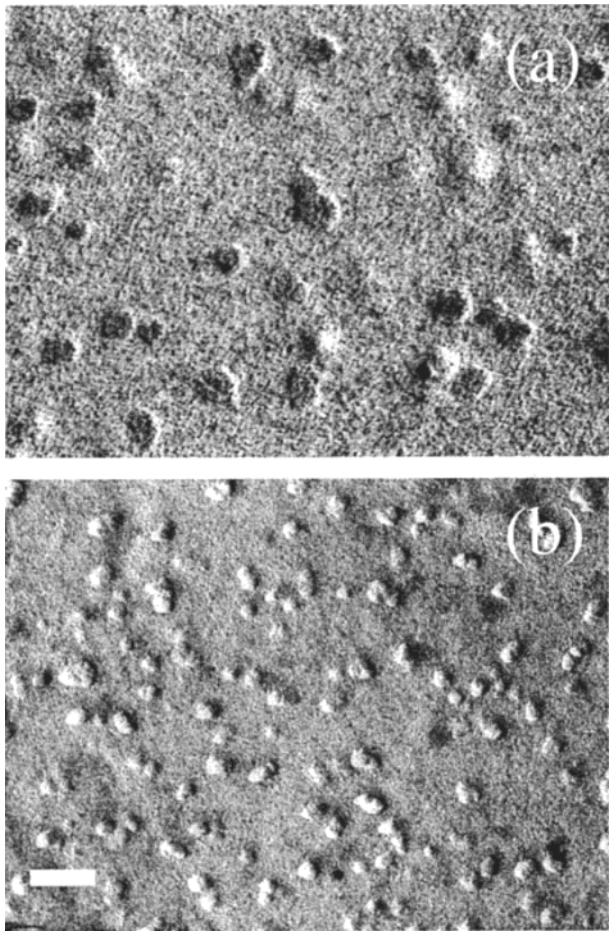


**Figure 2.** TEM replicas of PS-*b*-PA solutions with DN = 1 (a) and 0 (b). The DN = 1 sample was imaged directly, whereas the DN = 0 replica was obtained with freeze-fracture techniques. The bar corresponds to 100 nm.

**Neutron Data Analysis.** For simple salt-free solutions, all ions come from the copolymer, and there are four molecular components: solvent, the PS and PA blocks, and sodium counterions. The solvent is treated as a uniform background, and a description of the structure thus requires six partial structure factors. As judged from vapor pressure and sodium activity experiments, approximately 90% of the counterions is trapped within the corona (unpublished results). With X-ray reflectivity measurements it was shown that in a poly(ethylethylene-*block*-styrenesulfonate) monolayer at the air/water interface the majority of the counterions is bound to the polyelectrolyte block.[34] For a description of the scattering data, we assume that the distribution of the counterions along the radius equals the one for the PA monomers. This conjecture is recently confirmed by measuring the SANS of samples with isotopic labeling of the tetramethylammonium (TMA) counterions, while the contributions to the scattering related to the PA blocks are blanked with contrast matching in the water.[35] Accordingly, the polyelectrolyte block scattering length contrast has been calculated by taking the relevant average of the PAA and NaPA contrast parameters (see Table 2). The PS-*b*-PA solutions can be considered a two-component system, and the structure is given by three partial structure factors describing the density correlations among the PS (=*A*) and PA (=*B*) blocks.

The PS−PS, PA−PA, and PA−PA partial structure factors are obtained from the scattered intensities of

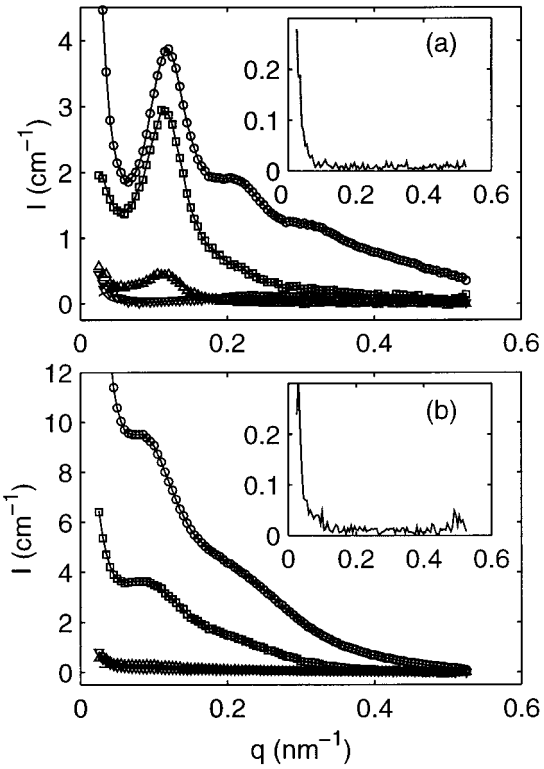


**Figure 3.** SANS intensity versus momentum transfer from 0.1 mol of PA/dm$^3$ PS-*b*-PA solutions with DN = 1 (a) and 0 (b). The $H_2O/D_2O$ composition is 99, 0, 28, and 47% $D_2O$ from top to bottom (for DN = 0 the intensities in 28 and 47% $D_2O$ are close). The lines represent a two-parameter fit in which the partial structure factors are optimized. The insets display the standard deviation of the two-parameter fit.

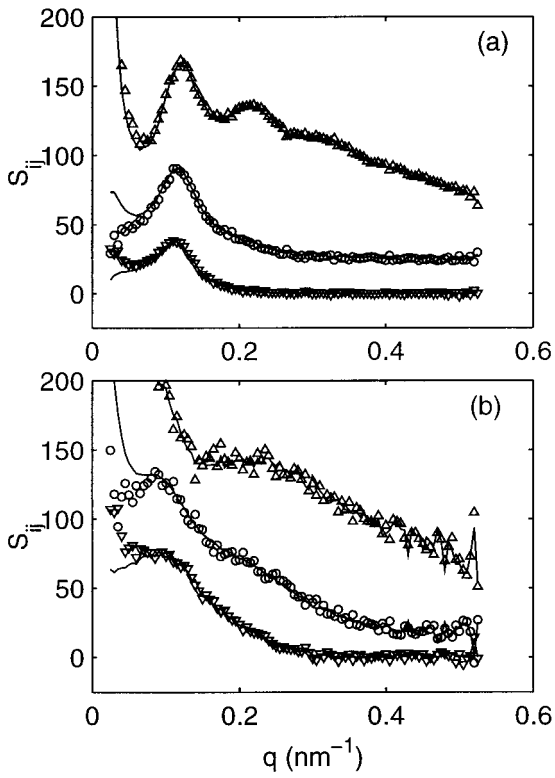


**Figure 4.** PS−PS (△), PS−PA (○), and PA−PA (▽) partial structure factors in 0.1 mol of PA/dm$^3$ PS-*b*-PA solutions obtained from a three-parameter fit. The solid curves result from a two-parameter fit. To avoid overlap, the PS−PA and the PS−PS partial structure factors are shifted upward by 25 and 50 units, respectively.

samples with different contrast length parameters. As an example, Figure 3 displays the intensities of fully neutralized (DN = 1) and nonneutralized (DN = 0) 0.1 mol of PA/dm$^3$ PS-*b*-PA solutions with contrast matching in water. The data collected in the low-$q$ region is displayed only. Note that in 28% $D_2O$ PS has negligible scattering length contrast, and the intensity is directly proportional to the PA structure factor. The scattering of the samples in $D_2O$ is the most intense due to the relatively large contrast length parameters. All samples show an upturn in intensity at low values of momentum transfer $q < 0.07$ nm$^{-1}$. The low-$q$ upturn is due to clustering (secondary aggregation) of block copolymer micelles, which was also indicated by static and dynamic light scattering (unpublished results). Furthermore, the intensities show a peak and oscillatory behavior at higher values of momentum transfer. This behavior is related to the ordering of the micelles and becomes more pronounced with increasing polyelectrolyte block charge. For low degrees of neutralization, the peak merges into the small-angle upturn and takes the form of a shoulder. These features will be discussed further on the following, when the experimental intensities are decomposed into the partial structure factors.

With four experimental intensities and three unknown partial structure factors, the data are overdetermined, and the partial structure factors can be derived by orthogonal factorization in a least-squares sense (i.e., a three-parameter fit to four data points for every $q$ value). In the data analysis, the degree of polymerization of the PS block was set to the value derived from the number-average molecular weight $M_n$ = 2000 quoted by the supplier ($N_{PS}$ = 20). However, for the PA block, use of the quoted molecular weight ($N_{PA}$ = 120) caused incorrect normalization of the PA−PA structure factor and incorrect limiting low-$q$ behavior of the composition structure factor (see below). Accordingly, $N_{PA}$ was optimized by satisfying the normalization constraints and takes the value 85 monomers per copolymer chain. Note that the manufacturer determined the degree of polymerization of the PA block from the ratio of the peak areas of the aromatic and aliphatic protons in the NMR spectrum of the poly(styrene-*b*-*tert*-butyl acrylate) precursor. (The PS block molecular weight was determined with size exclusion chromatography.) This NMR method is prone to error, because the peaks overlap due to the restricted segment mobility. The structure factors obtained from the intensities in Figure 3 are shown by the symbols in Figure 4. Note that the decomposition of the experimental intensities into the partial structure factors according to eq 1 is model-free; i.e., no assumptions regarding the morphology of the association structures have been made. As indicated by the electron micrographs, the micelles are spherical, irrespective of the degree of corona neutralization. Furthermore, due to the nonselective self-assembling process, the micelles are expected to be rather monodisperse in size. The statistical accuracy of the derived partial structure factors can be improved if the spherical shape of the micelles is recognized.

For monodisperse spherical micelles, the partial structure factors can be expressed as a product of terms involving the radial core and/or corona profiles and a term describing the micelle center-of-mass structure factor (eq 5). As shown by eq 8, the intensities can now be expressed in terms of two unknown factors $u_i(q)$

rather than three partial structure factors $S_{ij}(q)$ ($i, j$ = PS, PA). With a nonlinear least-squares procedure, the two factors $u_i(q)$ were fitted to the data, and the partial structure factors were reconstructed according to $S_{ij}(q) = u_i(q)u_j(q)$. The fitted intensities and the derived partial structure factors are given by the solid curves in Figures 3 and 4, respectively. The statistical accuracy in the structure factors has now improved. In the low-$q$ (upturn) region, the standard deviation of the fit (see insets of Figure 3) diverges, and the intensities do not comply with solvent composition independent structure factors. This shows that the samples differ in secondary aggregation, despite the fact that they have been prepared in the same way (but in various $H_2O/D_2O$ solvent ratios). For higher $q$ values, the standard deviation levels off, and the partial structure factors agree with the results obtained from the model-free three-parameter fit. Accordingly, it is assumed that for $q$ exceeding, say, 0.07 $nm^{-1}$ the data are not influenced by any residual clustering of micelles. Furthermore, the agreement between the results obtained with the two different fit procedures strongly supports our hypothesis that correlations between intermicelle separation and internal micelle structure can be neglected.

All of the data were analyzed with the two-parameter procedure, and similar agreement was observed (data not shown). The PS−PS (core) and PA−PA (corona) partial structure factors are shown in Figures 5 and 6, respectively. Both structure factors should extrapolate to the micelle aggregation number in the $q \rightarrow 0$ limit and the absence of intermicelle interference. The PS−PA cross partial structure factor is not displayed. Instead, the composition structure factor eq 4 is more informative and is displayed in Figure 7. The latter factor shows a maximum at wavelengths of the order of the inverse micelle radius. Furthermore, it approaches zero for $q \rightarrow 0$, because there can be no macroscopic phase separation of the chemically connected PS and PA blocks.

**Core Structure.** In Figure 5, the PS−PS partial structure factors are compared to the form factor of a uniformly dense sphere [i.e., according to eq 5 with the square of the relevant scattering amplitude eq 9 and $S_{cm}(q)$ set to unity]. The form factor was convoluted with a Gaussian resolution function with the wavelength spread and uncertainty in angle given in the Experimental Section.[36] In the low-$q$ range, the data deviate from the form factor, because of interference between cores pertaining to different micelles (see below). For $q$ exceeding, say, 0.15 $nm^{-1}$, the latter interference effects become progressively less important, and the structure factor reflects the internal structure of the core. In the double-logarithmic representation, the PS−PS partial structure factor displays an oscillation at $q \approx 1$ $nm^{-1}$. This feature corresponds with the (resolution broadened) first minimum and subsequent maximum in the sphere form factor and shows that the core is rather monodisperse in size. In the fit of the form factor, we have refrained from taking into account a polydispersity in core size. The fitted values of the core radius are approximately 4.5 nm and are collected in Table 3.

Another characteristic of the micelles is the aggregation number, i.e., the number of assembled copolymers per micelle. In the absence of intercore interference, the PS−PS structure factor is normalized to the aggregation number $N_{ag}$ at $q = 0$. In the comparison of the sphere form factor with the PS−PS data, $N_{ag}$ was optimized,

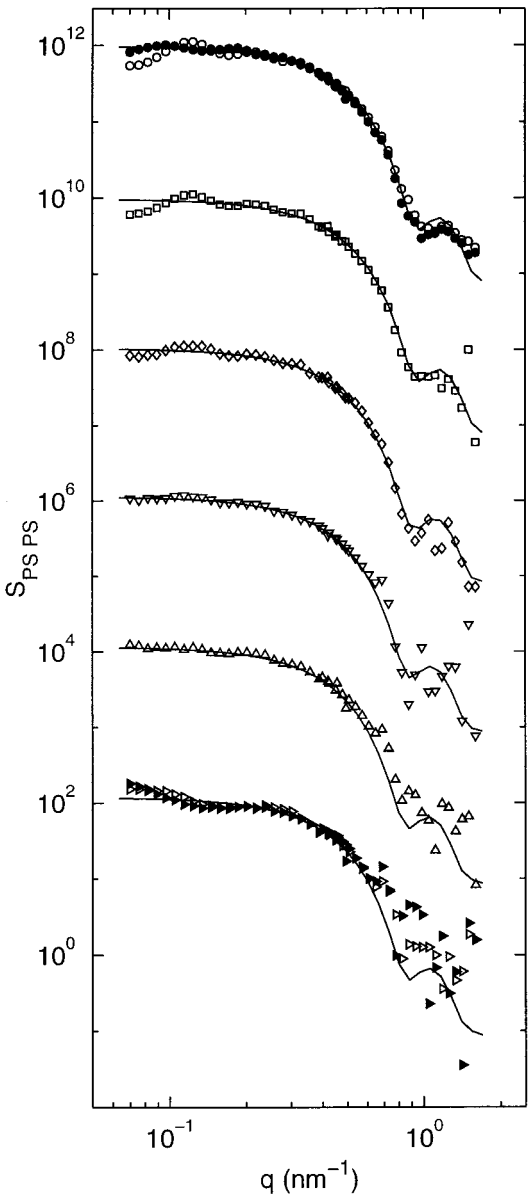


**Figure 5.** PS−PS partial structure factor versus momentum transfer: DN = 1 (○), 0.6 (□), 0.35 (◇), 0.1 (▽), 0.04 (△), and 0 (tilted △) from top to bottom. The data are shifted along the $y$-axis with an incremental multiplication factor. The polyelectrolyte block concentrations are 0.1 (open symbols) and 0.05 (closed symbols) mol of PA/$dm^3$. The curves represent a fit with the form factor of a uniform sphere.

and the resulting values are collected in Table 3. The aggregation number can also be derived from the size of the core and the PS block density $\rho_{PS}$ *inside* the core according to $N_{ag} = \rho_{PS} 4\pi r_c^3/3$. Provided the core is densely packed and solvent excluded, the block density within the core can be derived from the PS number-average molecular weight $M_n = 2000$ and the partial molar volume in Table 1. The resulting aggregation numbers are also collected in Table 3. In view of the uncertainty introduced by the intermicelle interference in the determination of $N_{ag}$ from the normalization of the structure factor, the agreement is gratifying. This confirms the PS block degree of polymerization $N_{PS} = 20$ and shows that the density inside the core is similar to the macroscopic value 1.05 kg/$dm^3$.

Both the core radius and aggregation number decrease with increasing degree of neutralization. How-

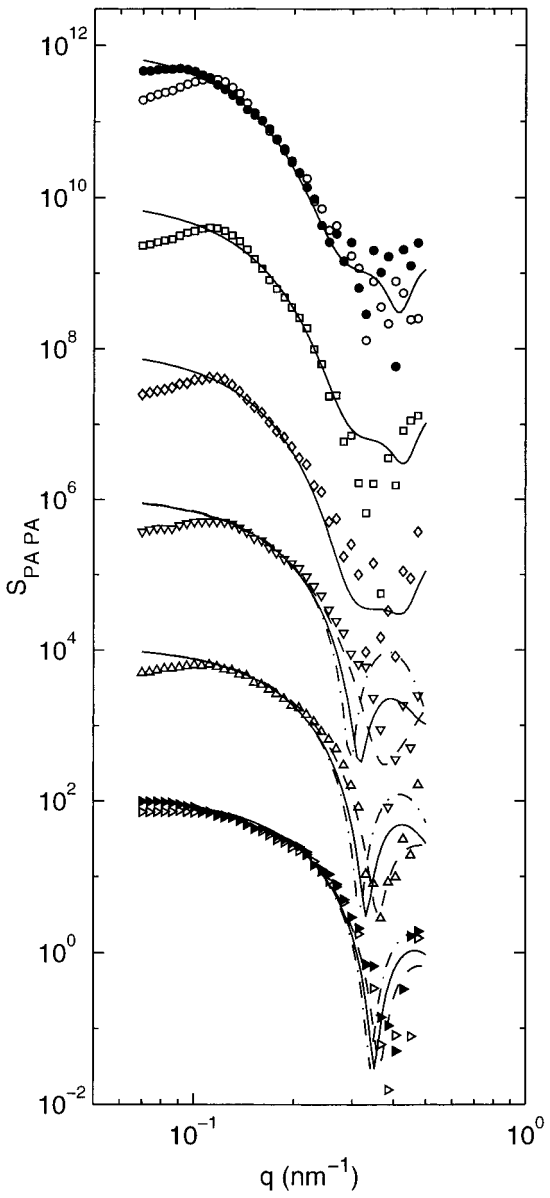


**Figure 6.** As in Figure 5, but for the PA−PA partial structure factor. The curves represent the PA form factor with corona density scaling exponent $\alpha = 2$ (solid), 1 (dashed−dotted), and $^8/_3$ (dashed). The curves with $\alpha = 1$ and $^8/_3$ are drawn for DN = 0, 0.04, and 0.1 only.

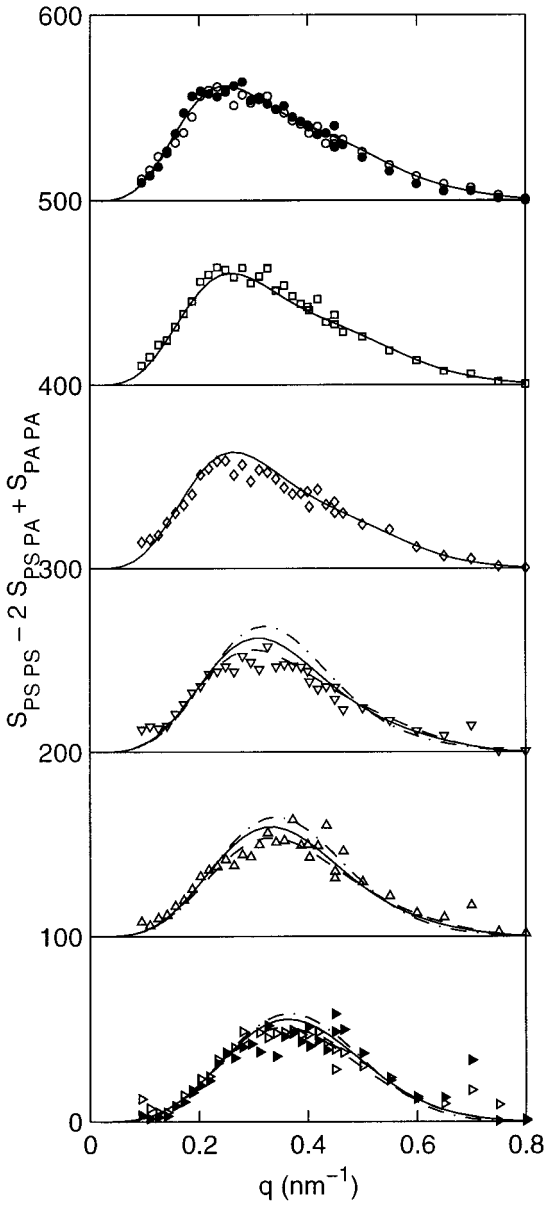


**Figure 7.** As in Figure 5, but for the PS−PS − 2 PS−PA + PA−PA composition structure factor. The curves represent the composition intramicelle form factor with corona density scaling exponent $\alpha = 2$ (solid), 1 (dashed−dotted), and $^8/_3$ (dashed). The data are shifted upward with an increment of 100 units.

ever, these effects are small and are of the order of the experimental error margins. It should be realized that the charge regulation and the measurements were done at room temperature, which is well below the glass temperature of PS (363 K). Accordingly, the core is in a glassy, metastable, state, and once the micelles are formed, the aggregation number is invariant to the corona charge and/or micelle concentration.

In the low-$q$ region, the PS−PS data deviate from the sphere form factor. With increasing degree of neutralization, a correlation peak with higher-order harmonics progressively develops at finite wavelengths. (The correlation peak is more clearly observed in Figure 4, which displays the low-$q$ region in the linear representation.) The position of this peak shifts to lower $q$ values with decreasing concentration according to $\rho^{1/3}$. A similar correlation peak is observed in the PA−PA partial structure factor (see Figure 4 and below). The peak position and its concentration scaling indicate that its origin is due to the ordering of the micelles, rather than correlations among copolymers within a single core. For

**Table 3. Polyelectrolyte Block Concentration, Degree of Neutralization DN, Aggregation Number $N_{ag}$, Core Radius $r_c$, and Outer Micelle Radius $r_o$[a]**

| concn (mol of PA/dm$^3$) | DN | $r_c$ (nm) | $N_{ag}^{I}$ | $N_{ag}^{II}$ | $r_o$ (nm) $\alpha = 1$ | $\alpha = 2$ | $\alpha = {}^8/_3$ |
|---|---|---|---|---|---|---|---|
| 0.093 | 1 | 4.48 | 109 | 97 | | 24 | |
| 0.046 | 1 | 4.48 | 109 | 98 | | 25 | |
| 0.093 | 0.6 | 4.52 | 112 | 97 | | 23 | |
| 0.093 | 0.35 | 4.52 | 112 | 104 | | 22 | |
| 0.093 | 0.1 | 4.51 | 111 | 114 | 16 | 18 | 20 |
| 0.093 | 0.04 | 4.56 | 115 | 116 | 15 | 16 | 17 |
| 0.093 | 0 | 4.56 | 115 | 119 | 13 | 14 | 15 |
| 0.046 | 0 | 4.56 | 115 | 119 | 13 | 14 | 15 |

[a] The aggregation number has been derived from (I) the core radius and (II) the normalization of the PS−PS partial structure factor.

the nonneutralized sample (DN = 0), a low-$q$ upturn in the PS−PS structure factor is observed due to secondary aggregation. However, a complete discussion of the intermicelle solution structure is beyond the scope of the present contribution. Here, we will further focus on the intramicelle structure, which is reflected by the corona PA−PA and the composition structure factors.

**Corona Structure.** For the different degrees of neutralization and micelle concentrations (DN = 0 and 1, only), the PA−PA partial structure factors are displayed in Figure 6. With decreasing degree of neutralization, the corona shrinks, and hence, the structure factor scales toward higher values of momentum transfer and the minimum at $q \approx 0.4$ nm$^{-1}$ becomes more pronounced (in the double-logarithmic representation). Furthermore, a correlation peak develops at finite wavelengths, which shifts to lower $q$ values with decreasing concentration according to $\rho^{1/3}$. This correlation peak is similar to the one observed in the core (PS−PS) structure factor and is due to the ordering of the micelles. For higher values of momentum transfer, the interference between different micelles becomes progressively less important, and the structure factors obtained for the two different copolymer concentrations superpose.

In the case of star-branched polyelectrolytes with a relatively small number of arms (∼12), a second correlation peak at higher values of momentum transfer has been reported.[37] The latter peak is due to fluctuations and correlations among the branches within a single star. For the copolymer micelles, the number of branches (i.e., the aggregation number) is much higher of the order of 100. The average segment density within the corona exceeds, say, 0.2 M. As judged from the position of the correlation peak in linear polyelectrolyte solutions at a comparable concentration, the corresponding intracorona correlation peak is expected at ∼0.7 nm$^{-1}$.[38] For such high values of momentum transfer the PA−PA structure factor is very small of the order of the experimental error margin (see Figure 6). Hence, the intracorona correlation peak and the effect of corona chain fluctuations are beyond detection. Furthermore, the micelle concentration is sufficiently low in the dilute regime such that the outer sections of the arms do not overlap. Accordingly, in the high-$q$ region the PA−PA structure factors may be compared with the corona form factor calculated with an average density profile eq 10.

The corona form factor was calculated with eq 5 (with $S_{cm}(q)$ set to unity) and the scattering amplitude eq 6 with numeric integration of the algebraic density profile eq 10. The results are displayed in Figure 6. Rather than optimizing the density scaling exponent α, the calculations were done with $\alpha = 2$ for all samples and $\alpha = 1$ and $^8/_3$ for DN = 0, 0.04, and 0.1 only. The value $\alpha = 2$ is relevant in the case of either full stretching of the chains or the formation of radial strings of blobs of uniform size. A density scaling exponent $\alpha = 1$ results from the Daoud−Cotton expanding blob model for uncharged star-branched polymers and α takes the value $^8/_3$ in the presence of charge annealing effects. The latter two values refer to Θ-solvent conditions; in a good solvent, the scaling exponent takes the values $^4/_3$ and $^5/_2$, respectively. Despite the fact that water is a good solvent for PA, we have used the Θ-solvent values because they are at the extremes of the range. In the calculation of the corona form factor, the outer micelle radius $r_o$ was optimized, whereas the aggregation numbers were fixed at their values obtained from the normalization of the PS−PS structure factor (Table 3). The micelle radius sets the scaling of the structure factor with momentum transfer. The fitted values of the micelle radius depend on the value of the density scaling exponent α and are listed in Table 3.

For a degree of neutralization exceeding, say, 0.35, an exponent $\alpha = 2$ gives nice agreement between the corona form factor and the data in the high-$q$ region where intermicelle interference becomes progressively less important. Although the scaling of the structure factors toward higher $q$ values with decreasing DN can be reproduced by a decrease in outer micelle radius, the results with $\alpha = 2$ fail to describe the position of the minimum at $q \approx 0.4$ nm$^{-1}$ for samples with low corona charge fraction. As can be seen in Figure 6, a Daoud−Cotton expanding blob model with $\alpha = 1$ shifts the minimum toward lower $q$ values and does not give a better agreement. Also, an analysis in terms of multiple scaling regimes pertaining to, e.g., expanding and constant blob size regions did not improve the description of the PA−PA structure factor. It is necessary to increase the density scaling exponent α beyond the value two in order to predict the position of the minimum correctly. Indeed, with $\alpha = ^8/_3$ nice agreement is observed, showing the importance of the dissociation and recombination balance of the weak polyacid (which results in a migration of the charges toward the outer corona region). With the good solvent value $\alpha = ^5/_2$ similar agreement is observed (results not shown). Further evidence for charge migration at low degree of neutralization will be presented in the following, when the composition structure factor is discussed.

**Block Ordering and Corona Expansion**. The composition structure factor eq 4 describes the spatial fluctuations of the blocks and is particularly sensitive to the intramicelle structure. The experimental results are displayed in Figure 7, together with the theoretical form factor expression eq 7 with $S_{cm}(q)$ set to unity. In the calculation of the composition form factor, the core and outer micelle radii, as well as the aggregation number, were fixed at their values obtained from the PS−PS (core) and PA−PA (corona) data (Table 3). In the long wavelength ($q \rightarrow 0$) limit, the composition structure factor goes to zero, which confirms the optimized PA block degree of polymerization $N_{PA}$. The theoretical form factor expression predicts the block ordering satisfactorily. In particular, deviations from the single-micelle calculation are less prominent in comparison with the situation for the PS−PS and PA−PA structure factors. This is because the composition structure factor takes its maximum value beyond the intermicelle correlation peak. In the region of the correlation peak (at $q \approx 0.12$ nm$^{-1}$), the composition factor already approaches zero due to the chemical attachment of the PA and the PS blocks.

The composition structure factor shows a maximum, which shifts toward smaller $q$ values with increasing degree of neutralization. This behavior is due to the expansion of the corona with increasing charge fraction and is reproduced in the form factor with a variation of the outer micelle radius. However, the calculated composition form factor with $\alpha = 2$ fails to describe the level of the maximum for samples with low corona charge fraction. As in the case of the PA−PA structure factor, for DN = 0, 0.04, and 0.1 the best agreement is observed

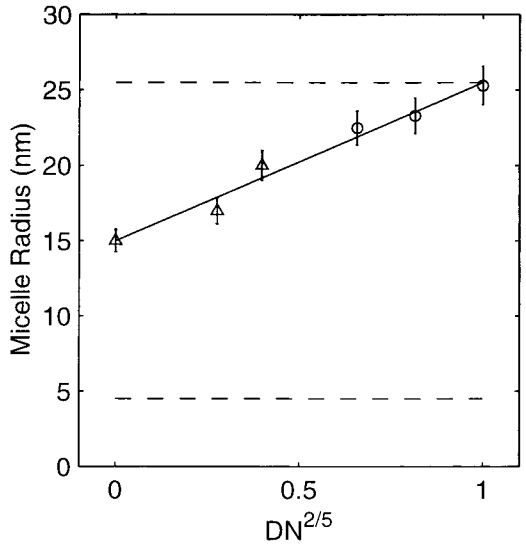


**Figure 8.** Micelle radius versus the scaled degree of neutralization calculated with corona density scaling exponent $\alpha = 2$ (○; DN = 0.35, 0.6, and 1) and $^8/_3$ (△; DN = 0, 0.04, and 0.1). The bottom and top dashed curves represent the core and fully expanded radii, respectively. The solid line denotes the scaling result for an osmotic salt-free polyelectrolyte star in a good solvent ($\nu = {}^3/_5$).

with $\alpha = {}^8/_3$ (with $\alpha = {}^5/_2$ similar agreement is observed; results not shown). The expanding blob model with $\alpha = 1$ results in a too high level of the maximum in the composition form factor. These results reinforce our conclusions concerning the importance of charge migration toward the outer corona region at low degrees of neutralization reached in the discussion of the corona structure.

With increasing charge fraction, the micelle radius first increases, subsequently levels off above 10% charge neutralization, and reaches the value 25 nm at full charge (Table 3 and Figure 8). The fully stretched value of the radius amounts 25.5 nm, as estimated from the sum of the core radius 4.5 nm and the contour length of the PA block (85 monomers per chain with a vinylic step length 0.25 nm). Accordingly, the NaPA chains in the coronas of the micelles take an almost fully stretched configuration at high pH and no added simple salt, as has been reported before in the literature.[10]

The expansion behavior can be rationalized with the scaling results for star-branched polyelectrolytes in the osmotic regime. According to eq 12 with $N_{ag} \sim 100$, the transition from the unscreened to the screened, osmotic, micelle occurs at a critical charge fraction $f_q \sim 10^{-4}$. Even the nonneutralized (DN = 0) micelle carries a sufficient amount of charge to retain the major part of its autodissociated protonic counterions inside the corona and, hence, is in the osmotic regime. For osmotic micelles, the micelle radius scales with the charge fraction according to $N_B a_B f_q^{1-\nu}$ (eq 13). To a good approximation, the charge fraction equals the degree of neutralization. Figure 8 displays the outer radius versus the scaled degree of neutralization with the good solvent value $\nu = {}^3/_5$. According to eq 13, there should be a linear dependence, which is indeed observed within the experimental accuracy. In the case of $\nu = {}^1/_2$, the agreement is somewhat worse, but the estimated error margins in the radii of the order of 5% do not allow an assessment of the solvent quality. Furthermore, in the present concentration range no significant change in micelle radius is observed.

## Conclusions

The degree of ionization in the coronal layer of spherical micelles of the polyacid diblock copolymer PS-*b*-PA can be tuned between almost zero and unity (where every segment carries a charge) by titration with alkali. With a view of describing the structural arrangement of the respective blocks, we have obtained the PS−PS, PA−PA, and the composition structure factors for samples with different degrees of ionization and/or copolymer concentration. The composition structure factor describes the correlation of the *difference* in density of the PS and PA blocks. All the structure factors are sensitive to interference between blocks pertaining to different micelles. In the composition structure factor, the latter effect is less prominent, because in the region of the correlation peak the composition structure factor already goes to zero due to the chemical attachment of the PS and the PA blocks. In the present contribution we have focused on the intramicelle structure; the correlation peak describes the organization among the micelles, and this part of the data still needs to be analyzed.

From the PS−PS structure factor, it was observed that the PS blocks form a spherical core. The aggregation numbers derived from the core size and the normalization of the structure factor are in reasonable agreement, which shows that the density inside the core is similar to the macroscopic polystyrene value. The dimension of the core and the aggregation number do not depend on the degree of ionization and/or copolymer concentration to a significant degree. This is perhaps not a surprising result because the core is in a glassy state, and during the experiments, the temperature was kept well below the glass temperature.

The structure factors that involve the PA block are sensitive to the density scaling and physical extent of the corona. At full ionization, a near 100% extension of the chains in the coronal layer is observed with a segment density scaling proportional to the inverse second power of the radius away from the core. At lower degrees of neutralization, the corona shrinks as manifested by, among others, a shift of the position of the maximum in the composition structure factor toward higher values of momentum transfer. Eventually, at very low charge fraction, the density scaling exponent has to be increased to a value around $^8/_3$ in order to get a satisfactorily agreement between the intramicelle form factor and the data. A value of the scaling exponent larger than two reflects a *decrease* in blob size with *increasing* distance away from the core. Such behavior can be rationalized in terms of a migration of the charges toward the outer region of the corona due to the dissociation and recombination balance of the weak polyacid.[27] We found no evidence for a Daoud−Cotton expanding blob region with a scaling exponent of the order of unity.[13] The absence of an expanding blob region is probably related to the presence of the core. In contrast to the situation for uncharged star-branched polymers, the grafting density at the core−corona interface sets a certain minimum blob size and limits the region over which the blobs are allowed to expand.

With an aggregation number of the order of 100, the majority of the counterions are either bound to the polyelectrolyte block or confined to the coronal layer. Accordingly, the scattering data could be consistently analyzed with the assumption that the counterion distribution along the radius equals the one for the PA

monomers in order to reduce the number of unknown structure factors. Recently, these conjectures were confirmed by a comparison of the counterion structure factors with those pertaining to the corona-forming PA blocks.[35] Another consequence of the trapping of the counterions is that the concomitant osmotic pressure gives the main contribution to the corona stretching force. Indeed, the derived dimension of the micelles as a function of the corona charge fraction complies with the scaling result for polyelectrolyte stars in the osmotic regime.[25,26] The sensitivity of the micelle structure to the corona charge fraction is strikingly different from the weak sensitivity to the addition of salt (charged brushes generate their own inner salinity by trapping of the counterions).[4,5,12,34] Accordingly, the feasibility to adjust the micelle dimension by variation of the corona charge fraction (e.g., by variation of the pH of the supporting buffer medium) rather than by variation of the ionic strength has considerable potential for applications.

**Acknowledgment.** We acknowledge the Laboratoire Léon Brillouin and Institute Max von Laue−Paul Langevin in providing the neutron research facilities. L. H. Leyte-Zuiderweg is thanked for IR spectroscopy. F. Spies and J. M. van't Noordende, Center for Electron Microscopy, Leiden University Medical Center, are acknowledged for recording the electron micrographs. J.vdM. has benefited from discussions with M. Daoud and M. Rawiso.

## References and Notes

(1) Zhang, L.; Eisenberg, A. *Science* **1995**, *268*, 1728.
(2) Moffitt, M.; Khougaz, K.; Eisenberg, A. *Acc. Chem. Res.* **1996**, *29*, 95.
(3) Cameron, N. S.; Corbierre, M. K.; Eisenberg, A. *Can. J. Chem.* **1999**, *77*, 7, 1311.
(4) Guenoun, P.; Davis, H. T.; Tirrell, M.; Mays, J. W. *Macromolecules* **1996**, *29*, 3965.
(5) Guenoun, P.; Delsanti, M.; Gazeau, D.; Mays, J. W.; Cook, D. C.; Tirrell, M.; Auvray, L. *Eur. Phys. J. B* **1998**, *1*, 77.
(6) Förster, S.; Hermsdorf, N.; Leube, W.; Schnablegger, H.; Regenbrecht, M.; Akari, S.; Lindner, P.; Böttcher, C. *J. Phys. Chem. B* **1999**, *103*, 6657.
(7) Regenbrecht, M.; Akari, S.; Förster, S.; Möhwald, H. *J. Phys. Chem. B* **1999**, *103*, 6669.
(8) Astafieva, I.; Zhong, X. F.; Eisenberg, A. *Macromolecules* **1993**, *26*, 7339.
(9) Astafieva, I.; Khougaz, K.; Eisenberg, A. *Macromolecules* **1995**, *28*, 7127.
(10) Zhang, L.; Barlow, R. J.; Eisenberg, A. *Macromolecules* **1995**, *28*, 6055.
(11) Here, $q$ denotes the momentum transfer and is defined by the wavelength $\lambda$ of the radiation and the angle $\theta$ between the incident and scattered beam according to $q = 4\pi/\lambda \sin(\theta/2)$.
(12) Guenoun, P.; Muller, F.; Delsanti, M.; Auvray, L.; Chen, Y. J.; Mays, J. W.; Tirrell, M. *Phys. Rev. Lett.* **1998,** *81*, 3872.
(13) Daoud, M.; Cotton, J.-P. *J. Phys. (Paris)* **1982,** *43*, 531.
(14) Dozier, W. D.; Huang, J. S.; Fetters, L. J. *Macromolecules* **1991**, *24*, 2810.
(15) Cogan, K. A.; Gast, A. P.; Capel, M. *Macromolecules* **1991**, *24*, 6512.
(16) Förster, S.; Wenz, E.; Lindner, P. *Phys. Rev. Lett.* **1996**, *77*, 95.
(17) Marques, C. M.; Izzo, D.; Charitat, T.; Mendes, E. *Eur. Phys. J. B* **1998**, *3*, 353.
(18) Lovesey, S. W. *Theory of Neutron Scattering from Condensed Matter*; Oxford University Press: Oxford, 1984; Vol. 1.
(19) Higgins, J. S.; Benoit, H. C. *Polymers and Neutron Scattering*; Oxford University Press: Oxford, 1994.
(20) Rawiso, M. *J. Phys. IV* **1999**, *9*, Pr1−147.
(21) Israëls, R.; Leermakers, F. A. M.; Fleer, G. J. *Macromolecules* **1994**, *27*, 3087.
(22) Israëls, R.; Leermakers, F. A. M.; Fleer, G. J.; Zhulina, E. B. *Macromolecules* **1994**, *27*, 3249.
(23) Lyatskaya, Yu. V.; Leermakers, F. A. M.; Fleer, G. J.; Zhulina, E. B.; Birshtein, T. M. *Macromolecules* **1995**, *28*, 3562.
(24) Shusharina, N. P.; Nyrkova, I. A.; Khokhlov, A. R. *Macromolecules* **1996**, *29*, 3167.
(25) Misra, S.; Mattice, W. L.; Napper, D. H. *Macromolecules* **1994**, *27*, 7090.
(26) Borisov, O. V. *J. Phys. II* **1996**, *6*, 1.
(27) Borisov, O. V.; Zhulina, E. B. *Eur. Phys. J. B* **1998**, *4*, 205.
(28) Note that this definition differs from the situation for homopolymers, where the monomer is usually considered to be the elementary scattering unit.
(29) Pedersen, J. S.; Gerstenberg, M. C. *Macromolecules* **1996**, *29*, 1363.
(30) Förster, S.; Burger, C. *Macromolecules* **1998**, *31*, 879.
(31) Auvray, L. *C. R. Acad. Sci. Paris* **1986**, *302*, 859.
(32) Auvray, L.; de Gennes, P. G. *Europhys. Lett.* **1986**, *2*, 647.
(33) This value was obtained from the experimental p$K$ = 7.2 of simple salt-free 0.014 mol of PA/dm$^3$ PS-*b*-PA solutions, unpublished results.
(34) Ahrens, H.; Förster, S.; Helm, C. A. *Phys. Rev. Lett.* **1998**, *81*, 4172.
(35) Groenewegen, W.; Lapp, A.; Egelhaaf, S. U.; van der Maarel, J. R. C., submitted for publication.
(36) Pedersen, J. S. *J. Phys. IV* **1993**, *3*, 491.
(37) Heinrich, M.; Rawiso, M.; Zilliox, J. G.; Lesieur, P.; Simon, J. P. *Eur. Phys. J. E*, in press.
(38) van der Maarel, J. R. C.; Groot, L. C. A.; Hollander, J. G.; Jesse, W.; Kuil, M. E.; Leyte, J. C.; Leyte-Zuiderweg, L. H.; Mandel, M.; Cotton, J.-P.; Jannink, G.; Lapp, A.; Farago, B. *Macromolecules* **1993**, *26*, 7295.
(39) Hiraoka, K.; Yokoyama, T. *J. Polym. Sci., Polym. Phys.* **1986**, *24*, 769.

MA992116P